J. Fluid Mech. (2013), *vol.* 735, *pp.* 587–612. © Cambridge University Press 2013
doi:10.1017/jfm.2013.519

Three-dimensional flow within shallow, narrow cavities

Sarah D. Crook[1], Timothy C. W. Lau[2,†] and Richard M. Kelso[2]

[1]Nova Systems, Edinburgh, SA 5111, Australia

[2]Centre for Energy Technology, School of Mechanical Engineering, The University of Adelaide, SA 5005, Australia

(Received 17 February 2013; revised 15 August 2013; accepted 25 September 2013; first published online 28 October 2013)

The three-dimensional structure of incompressible flow in a narrow, open rectangular cavity in a flat plate was investigated with a focus on the flow topology of the time-averaged flow. The ratio of cavity length (in the direction of the flow) to width to depth was $l{:}w{:}d = 6{:}2{:}1$. Experimental surface pressure data (in air) and particle image velocimetry data (in water) were obtained at low speed with free-stream Reynolds numbers of $Re_l = 3.4 \times 10^5$ in air and $Re_l = 4.3 \times 10^4$ in water. The experimental results show that the three-dimensional cavity flow is of the 'open' type, with an overall flow structure that bears some similarity to the structure observed in nominally two-dimensional cavities, but with a high degree of three-dimensionality both in the flow near the walls and in the unsteady behaviour. The defining features of an open-type cavity flow include a shear layer that traverses the entire cavity opening ultimately impinging on the back surface of the cavity, and a large recirculation zone within the cavity itself. Other flow features that have been identified in the current study include two vortices at the back of the cavity, of which one is barely visible, a weak vortex at the front of the cavity, and a pair of counter-rotating streamwise vortices along the sides of the cavity near the cavity opening. These vortices are generally symmetric about the cavity centre-plane. However, the discovery of a single tornado vortex, located near the cavity centreline at the front of the cavity, indicated that the flow within the cavity is asymmetric. It is postulated that the observed asymmetry in the time-averaged flow field is due to the asymmetry in the instantaneous flow field, which switches between two extremes at large time scales.

Key words: aerodynamics, flow–structure interactions

1. Introduction

Flows past cavities, gaps and steps are of interest to researchers because these features are found on nearly all vehicles. Rich, complex fluid dynamics are associated with these geometrically simple objects. Two examples are the gaps in external car rear-view mirrors and the cavities in modern aircraft (e.g. weapon bays). In the latter, the cavities produce increased aerodynamic drag and significant acoustic emissions. During high speed subsonic flight, flow oscillations in aircraft cavities are particularly violent and can generate noise levels in excess of 180 dB and vibration loads that

† Email address for correspondence: timothy.lau@adelaide.edu.au

https://doi.org/10.1017/jfm.2013.519 Published online by Cambridge University Press

can damage sensitive equipment or even cause catastrophic failure of the airframe components.

There is a wealth of literature in the area of cavity flows, ranging from early fundamental studies by Karamecheti (1956), Plumblee, Gibson & Lassiter (1962), Rossiter (1964) and East (1966), to detailed computational simulations by Larsson (2002), Yao, Cooper & Raghunathan (2004), Larcheveque *et al.* (2004) and Mary & Le (2005). Due to the severity of the problems associated with aircraft cavity flow, much of the early work has been carried out at flow speeds comparable to aircraft operational speeds. As a result, the majority of the research focuses on the two-dimensional flows in the transonic-to-supersonic flow regime (e.g. Stallings & Wilcox 1987; Dix & Butler 1990; Tracy & Plentovish 1993; Forestier, Jacquin & Geffory 2003; Ashcroft & Zhang 2005), leaving the area of low speed three-dimensional cavity flows relatively unexplored. These two-dimensional models and flow descriptions are valuable as fundamental studies, but these descriptions are inadequate to explain the complex topology of three-dimensional cavity flows. Due to the complexity of the flow in and around three-dimensional cavities and the difficulty in obtaining reliable data in such highly turbulent flows, experimental investigations in this area have largely given way to computational simulations.

There exists only a handful of published work that investigates the flow topology within a three-dimensional cavity. Notable publications include Wilcox (1992), Dolling, Perng & Leu (1997), Larcheveque, Sagaut & Labbe (2007), Knowles, Ritchie & Lawson (2007) and Atvars *et al.* (2009). Furthermore, there appears to be a shortage of literature in low speed cavity flows (Sarohia 1977; Milbank 2004; Ozsoy *et al.* 2005; Manovski, Giacobello & Soria 2008). Although many breakthroughs have been made, the fundamental flow topology of low speed, three-dimensional cavity flows has not yet been mapped. The aim of this study is, therefore, to provide an extensive description of the time-averaged three-dimensional structure of incompressible flow in an open rectangular cavity in a flat plate.

The experiment consists of two parts. First, measurements of the surface pressure distribution within the cavity in air are performed. Second, the velocity field in and near the cavity is obtained by particle image velocimetry (PIV) in water. The results obtained from both parts are then used together to infer the complex topology of the flow.

1.1. *General description of cavity flows*

Simple cavities are typically described as rectangular, with a particular length l, width w and depth d (see figure 1). The non-dimensional parameter l/d is of particular importance, as it has been found that significantly different flow regimes exist depending on this ratio (Charwat *et al.* 1961; Sarohia 1977; Stallings & Wilcox 1987; Ashcroft & Zhang 2005). At subsonic flow speeds, an 'open-type' flow field exists for $l/d \lesssim 6$–7. An open-type flow field is characterized by a shear layer that bridges the entire cavity opening, and by a large recirculation zone inside the cavity itself (see figure 2). For $l/d \gtrsim 8$–9, the shear layer generated at the front of the cavity reattaches on the bottom of the cavity, and no large recirculation zone exists in the centre of the cavity. This flow regime is called a 'closed-type' cavity flow. In between these two ranges, a transitional regime exists.

For open-type cavity flows, other flow features have also been identified in previous studies. In a study utilizing flow visualization and surface pressure measurements within a hypersonic cavity flow at $Re = 5 \times 10^7$, Dolling *et al.* (1997) report that aside from the large recirculation zone, two other vortical structures exist within the cavity.

https://doi.org/10.1017/jfm.2013.519 Published online by Cambridge University Press

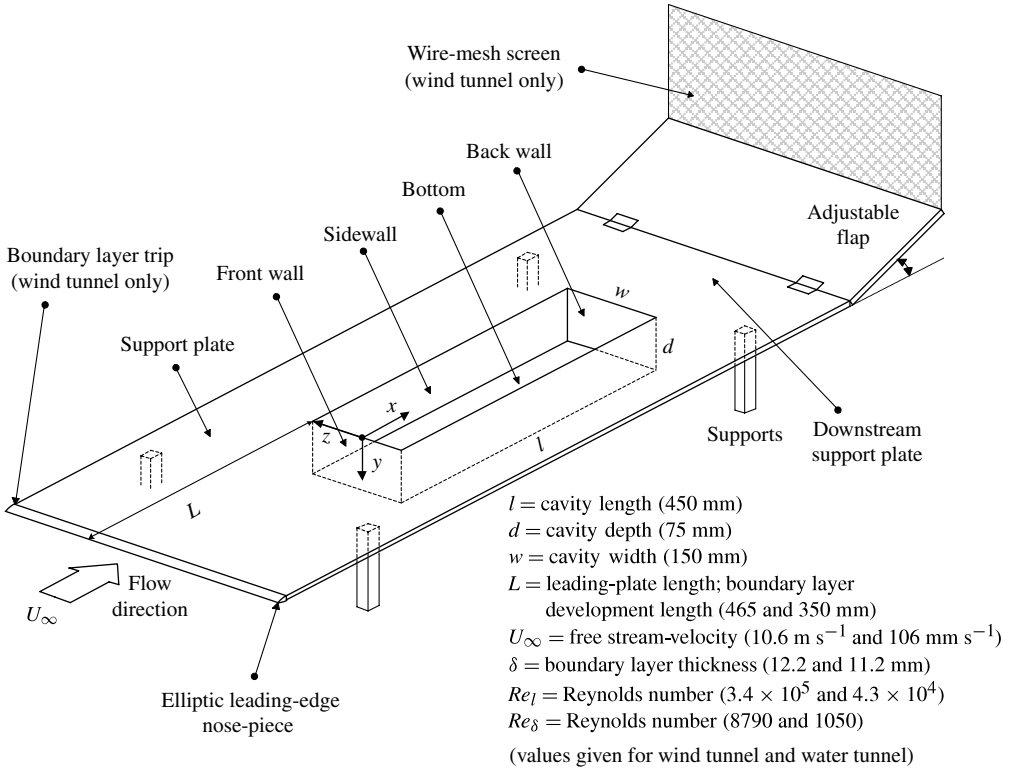


FIGURE 1. Illustration of cavity model with nomenclature, coordinate system and commonly used flow parameters (air and water respectively).

Firstly, a vortex was observed close to the junction between the back wall and bottom of the cavity. This rear corner vortex was reported to have very small dimensions relative to cavity, and to have opposite rotational sense to that of the recirculation vortex. Dolling *et al.* postulate that this vortex entrains mass from the recirculation vortex and transports this mass to the front of the cavity. Secondly, a weak (in terms of circulation) vortex of the same rotational direction to the recirculation zone was observed at the front of the cavity. Flow visualization of wide cavities (l:w:d = 2:6:1) at the lower Reynolds numbers of $Re \approx 2.3$–5.3×10^3 by Faure *et al.* (2007) agree with these observations.

However, the existence of both the front and the small rear corner vortices are not consistently observed in all cavity flows. For example, in a numerical study by Zdanski *et al.* (2003) on cavities with variable $l/d = 6$–8 at $Re \approx 1.8 \times 10^4$, the recirculation zone was seen to extend all the way upstream to the front of the cavity. No front vortex was observed. However, in the case where $l/d = 8$, the small rear corner vortex was observed. In numerical studies of very wide cavities (l:w:d = 4:12:1) at low $Re = 3 \times 10^3$, Yao *et al.* (2004) showed that the flow within the cavity consists of a large recirculation zone only. No other flow structures were evident in the cavity cross-sectional plane. In an investigation of a nominally two-dimensional cavity flow using PIV in a wind tunnel, Ashcroft & Zhang (2005) observed the front vortex at the junction between the front and bottom of the cavity. The strength and size of the front vortex varied depending on the location and size of the recirculation zone. The

https://doi.org/10.1017/jfm.2013.519 Published online by Cambridge University Press

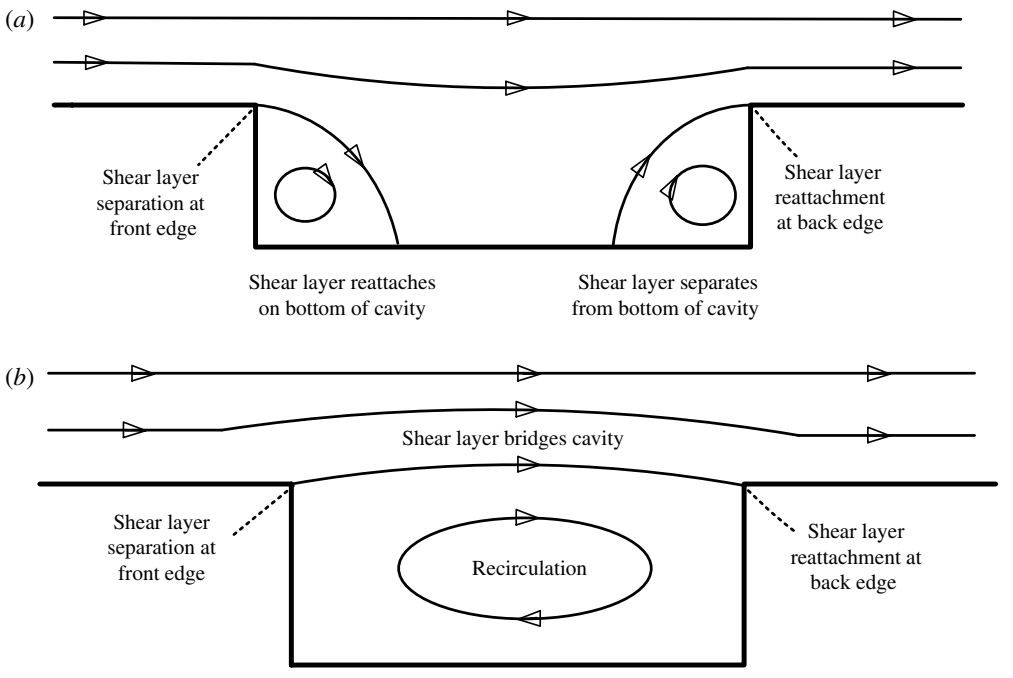


FIGURE 2. Two-dimensional representation of (*a*) closed-type cavity flow and (*b*) open-type cavity flow.

front corner vortex was seen to be largest in the longest cavity investigated, as a result of increased distance to the centre of the recirculation zone. Knowles *et al.* (2007) studied the flow within a cavity of dimensions $l{:}w{:}d = 5{:}2{:}1$ at transonic flow speeds and high $Re = 1.3 \times 10^7$, and observed a single recirculation zone that occupied the entire cavity. No other structures were reported. Flow visualization of a similar cavity by Atvars *et al.* (2009) reveals that a small rear corner vortex exists in the cavity which was not apparent in the computational results.

The observations of the two-dimensional cavity flow along the cavity centre-plane are summarized in figure 3. The defining features of an open-type cavity flow is a shear layer that traverses the entire cavity opening and impinges on the back wall of the cavity, as well as a large recirculation zone that encompasses most of the internal cavity. As discussed above, a weak front vortex may also be present, rotating in the opposite direction to the recirculation zone. At the junction of the cavity back wall and bottom surface, a very small rear corner vortex may also be present.

While it is useful to have a general, two-dimensional description of cavity flows, there is evidence that these flows are highly three-dimensional, even for very wide cavities. For example, utilizing oil flow visualization of relatively wide cavities ($l{:}w{:}d = 2{:}1$–$8{:}18$), Maull & East (1963) observed that the spanwise line separating the front vortex from the recirculation zone along the bottom of the cavity was neither straight nor symmetric about the centre-plane. In a numerical study by Yao *et al.* (2004), the fluid flow within the recirculation zone was found to be highly three-dimensional and unsteady, evidenced by transient longitudinal vortices transporting fluid across the width of the cavity. In contrast, large-eddy simulations have indicated that while the front vortex is strongly asymmetric, the main recirculation zone is

https://doi.org/10.1017/jfm.2013.519 Published online by Cambridge University Press

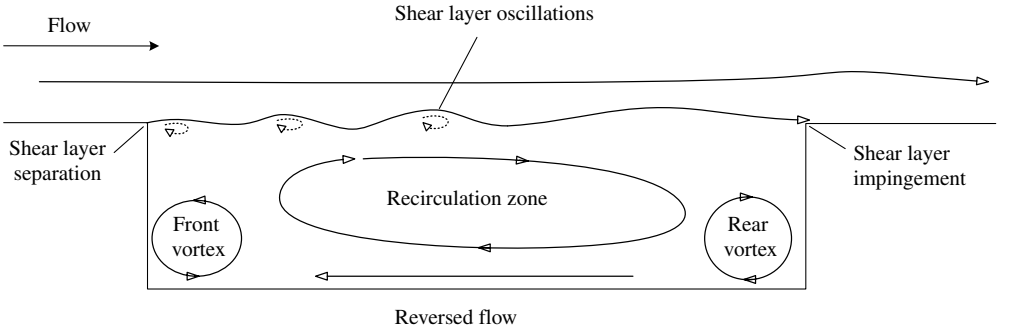


FIGURE 3. Illustration of typical flow features observed in two-dimensional cavities, based on existing literature.

relatively symmetric about the cavity centre-plane (Larcheveque *et al.* 2007). Flow visualization of wide cavities at low Reynolds numbers have also indicated that the interaction between the recirculation and front vortices causes spanwise flow near the front corner of the cavity opening, suggesting flow structures that appear to be two-dimensional may also have three-dimensional effects (Faure *et al.* 2007).

A series of in-depth and detailed investigations were carried out by Stallings & Wilcox (1987) and later Wilcox (1990) on the three-dimensional pressure distributions in a variety of cavity configurations at supersonic speeds. They found that three-dimensional effects in the form of large lateral pressure gradients occurred on the back wall. The gradients were generally symmetric about the cavity centre-plane for closed cavity flows but in some cases were asymmetric for the open-cavity case. The large pressure gradients and the location of the peak pressures were thought to be associated with the impingement of the shear layer vortices on the back wall. In a similar study, Mary & Le (2005) suggested that the three-dimensional nature of the flow field in wide cavities may be due to turbulence or asymmetries in the cavity geometry. These findings suggest that the cavity flows are three-dimensional, even for very wide cavities.

2. Experimental equipment and technique

The three-dimensional cavity flow experiments consisted of pressure measurements in air and PIV in water. These experiments required the use of two separate, but similar, cavities. One cavity was designed for use in air, and was therefore fabricated with pressure tappings, while the other cavity was for use in the water experiments, and was therefore designed to maximize optical access. Apart from the lengths of the leading flat plate and the rear adjustable flap, the two cavities were geometrically similar. The leading edge of the flat plate had an elliptical profile in accordance with Thwaites' analysis to avoid flow separation (Thwaites 1949). The design of the cavity is shown in figure 1. The length:width:depth ratio of the cavity is $l{:}w{:}d = 6{:}2{:}1$, and therefore this cavity should experience an open-type flow field (Charwat *et al.* 1961; Sarohia 1977; Stallings & Wilcox 1987).

While the pressure and PIV measurements were performed at different Reynolds numbers, i.e. $Re_l = 3.4 \times 10^5$ and $Re_l = 4.3 \times 10^4$ respectively, the effect of the Reynolds number on the mean flow measurements is expected to be small (Rossiter 1964; Tracy & Plentovish 1993). However, it has been found that one of the primary

https://doi.org/10.1017/jfm.2013.519 Published online by Cambridge University Press

parameters that must be matched to achieve similarity in open-type cavities is the boundary layer thickness (Rossiter 1964). Therefore, both experiments were designed to achieve similar boundary layer thicknesses, as discussed in detail in the following section.

2.1. *Apparatus for experiments in air*

The experiments in air consisted of pressure measurements along the surface of the cavity. These experiments were conducted in a wind tunnel which has a closed-return test section and is driven by an axial-flow fan. The tunnel has a 4:1 area ratio contraction (octagonal to square) with three flow-conditioning screens installed before the contraction. The wind tunnel contraction exit has a cross-section area of 0.5 m $\times$ 0.5 m, and the test section has a length of 3 m. With the cavity installed, the spanwise variation in the free-stream velocity upstream of the cavity is 0.66 %. Utilizing hot-wire anemometry, the wind-tunnel turbulence intensity was measured to be 0.8 % at a free-stream velocity of 25 m s^{-1}.

To ensure that the boundary layer thickness in both the air and water experiments were approximately the same, a boundary layer trip was employed in the air experiments. The trip consisted of a 0.4 mm diameter wire located 40 mm downstream of the flat plate leading edge. The boundary layer trip diameter was selected based on guidelines published in Braslow, Hicks & Harris (1966).

Surface pressure measurements were obtained from flush-mounted pressure tappings on the surfaces of the cavity and on the flat plate. One half of the cavity was fully instrumented and a number of additional ports were installed on the other half to detect any asymmetry in the pressure field. The entire cavity contained 191 pressure tappings. Figure 4 shows the location of the tappings (excluding a small number on the leading plate). The separation between tappings depended on the expected spatial variation in surface pressure. In regions where high pressure gradients were expected, the pressure tappings were located closer together.

Each pressure tapping had an internal diameter of 0.4 mm at the surface and was flush and square with the surface. The pressure tappings were individually selected for measurement using a modified SS3-48 Scanivalve multiplexer. All pressures were measured on a 10 Torr MKS Baratron and the output was recorded using a National Instruments USB-6009 Data Logger. The frequency response of the Baratron was approximately 0.25 Hz. Each port was sampled at a rate of 1000 Hz for a sampling time of 60 s. The pressure measurements were repeated three times on separate days to ensure repeatability. There were negligible differences between the data taken across the three days. The three sets of data were combined into a single set.

The pressure readings, P, were time-averaged and then normalized by the free-stream dynamic pressure, giving non-dimensional pressure coefficients $C_p = \overline{P}/(1/2\rho U_\infty^2)$ at each tapping location. The standard deviation (with respect to time), σ_P, was also calculated at each location.

The experiments were performed at a fixed free-stream speed of 10.6 m s^{-1}, corresponding to a Reynolds number of $Re_l = 3.4 \times 10^5$. The boundary layer thickness, measured on the cavity centreline at the front corner of the cavity, was $\delta_{air} \approx 12.2$ mm. The boundary layer shape factor, $H = \delta^*/\theta$, where δ^* is the displacement thickness and θ is the momentum thickness, for the experiments in air was calculated as $H_{air} = 1.41$. This suggests that the boundary layer was turbulent.

The experimental errors, estimated from measurements of the pressure fluctuations in the absence of a free stream, were approximately ± 2.5 %.

https://doi.org/10.1017/jfm.2013.519 Published online by Cambridge University Press

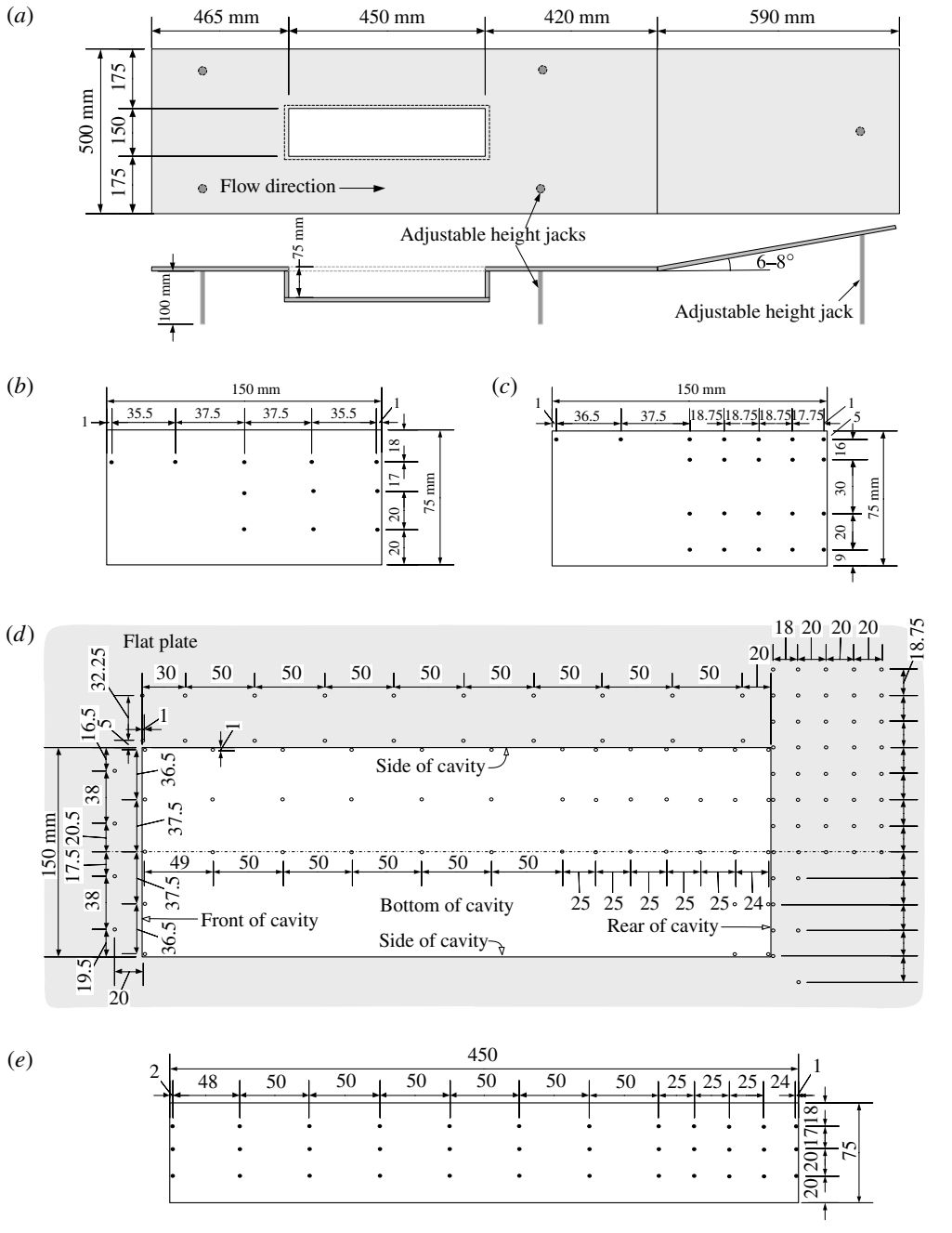


FIGURE 4. Location of surface pressure tappings in the flat plate and cavity, air flow model only. All dimensions are in mm. (*a*) Top view and side view of flat plate, cavity and adjustable flap. (*b*) Front wall (11 ports): view from downstream. (*c*) Back wall (22 ports): view from downstream. (*d*) Pressure ports on support plate (71 ports) and bottom of cavity (45 ports): top view. (*e*) Sidewall (36 ports).

https://doi.org/10.1017/jfm.2013.519 Published online by Cambridge University Press

2.2. *Apparatus for experiments in water*

The experiments in water were conducted in a closed-return free-surface water channel with a variable-speed pump and 4:1 three-dimensional contraction. The tunnel has a 2 m long test section, with a 0.5 m × 0.5 m cross-section (same as the wind tunnel). The flow was seeded with hollow glass spheres of mean diameter 8 μm.

Illumination for the PIV measurements was provided by a dual-cavity frequency-doubled Quantel Brilliant B Twins Nd:YAG laser. This laser produces monochromatic light at a wavelength of 532 nm at a fixed pulse frequency of 10 Hz. The laser power was measured as ≈180 mJ per pulse. The laser beam was formed into a sheet via a series of mirrors and shaping optics. PIV images were recorded by a Kodak Megaplus ES 1.0 10-bit CCD camera with a Nikon 70–300 mm zoom lens.

The PIV setup was configured to provide planar velocity measurements in three separate, mutually orthogonal orientations (see figure 5). To observe small features of the flow, the size of the imaging region was set significantly smaller than the length of the cavity. This required the use of multiple measurement windows, as shown in figure 6. In summary, the measurements consist of the following:

(i) Streamwise and normal components of velocity (u, v) in three x–y planes at $z/d = 0$ (centre), $z/d = 0.5$ (quarter-width) and $z/d = 0.98$ (near sidewall). For each plane, seven separate, overlapping windows were used.

(ii) Streamwise and transverse components of velocity (u, w) in four x–z planes with their locations (depths) selected based on results obtained from the x–y plane. The planes consist of $y/d = -0.03$ (above the cavity and to the side), $y/d = 0.15$ (below the cavity opening and approximately level with the shear layer stagnation on the back wall), $y/d = 0.70$ (approximately level with the centre of the rear vortex and front vortex) and $y/d = 0.97$ (close to the bottom of the cavity). The plane at $y/d = -0.03$ was measured using 14 separate windows (arranged in a 7 × 2 grid), while the remaining three x–z planes were measured using five separate measurement windows.

(iii) Normal and transverse components of velocity (v, w) in 10 y–z planes spaced from the front wall to the back wall of the cavity every 50 mm (except at $x = 100$ mm due to an optical obstruction).

Each overlapping image was obtained by shifting the cavity forwards into position and maintaining the same laser and camera setup. In the y–z plane, overlapping images were not required and the cavity was shifted downstream to obtain several independent cross-sectional images of the flow. To ensure that the circulation around the plate, and hence the stagnation of the flow on the leading edge, did not change during the shift, the stagnation streakline was observed at every cavity location.

Interrogation-window sizes of 32×32 pixels and 16×16 pixels were used (depending on the measurement plane), each with a 50 % overlap. Correlation peaks were detected using a multi-pass double correlation, least-squares Gaussian fit.

For each measurement window, a total of 1150 vector fields were obtained. These fields were then averaged to produce a time-averaged velocity field. Anomalous velocity vectors (outliers) were detected using the universal median technique of Westerweel & Scarano (2005). Detected outliers were replaced with a weighted average of valid surrounding vectors. When several of the immediate neighbours were also outliers then a Gaussian-weighted interpolation scheme was used.

The experiments in water were performed at a fixed free-stream velocity of $U_\infty = 106$ mm s^{-1}, corresponding to a Reynolds number of $Re_l = 4.3 \times 10^4$. The boundary layer thickness was measured to be $\delta_{water} \approx 11.2$ mm. The boundary layer

https://doi.org/10.1017/jfm.2013.519 Published online by Cambridge University Press

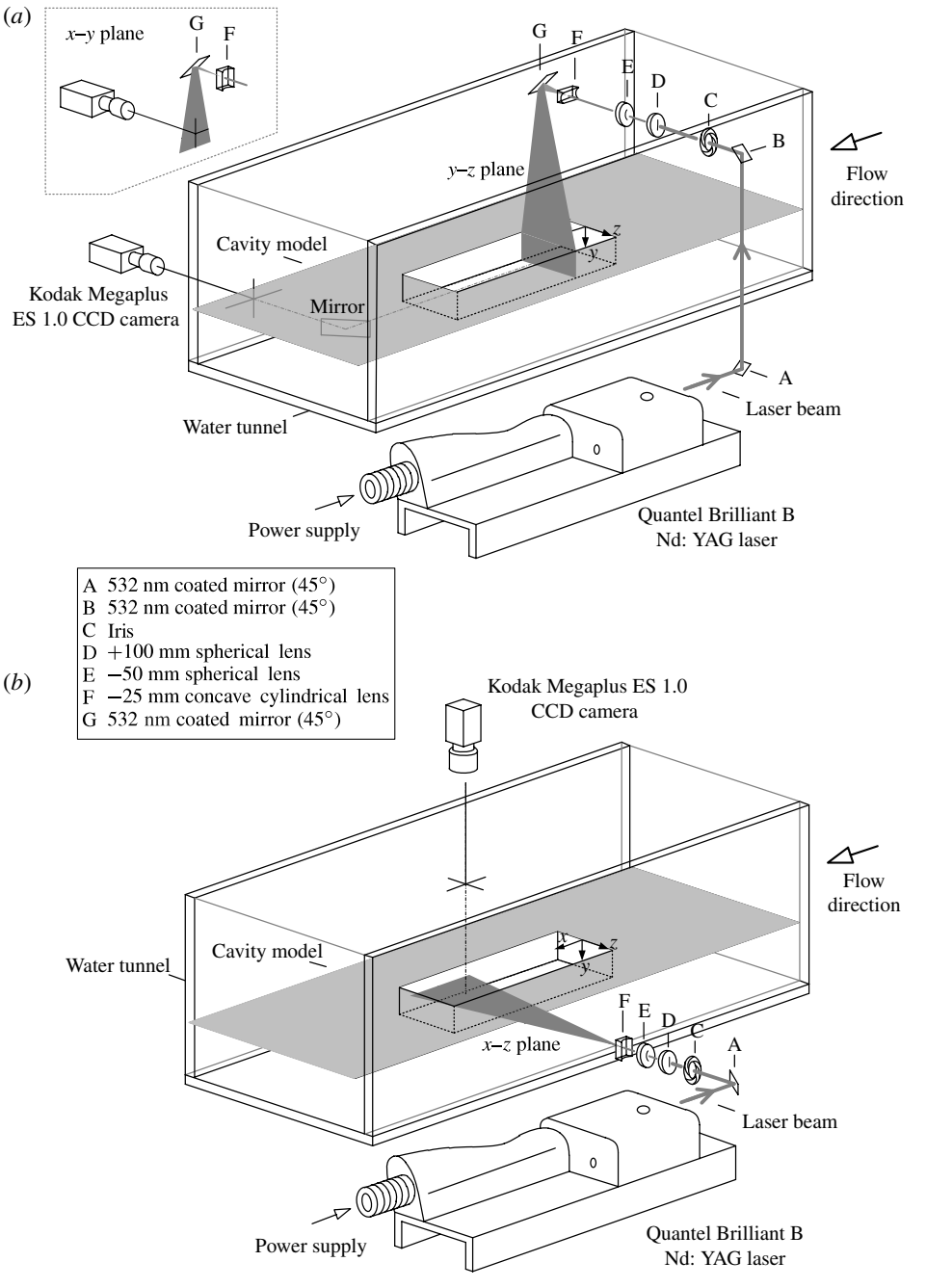


FIGURE 5. PIV setup: (*a*) inset *x*–*y* plane, main figure *y*–*z* plane; (*b*) *x*–*z* plane.

thicknesses in both the air and water experiments were therefore similar. However, the boundary layer shape factor for the experiments in water was calculated as $H_{water} = 2.48$, implying that the boundary layer was laminar. The boundary layer types in the experiments in water and air were therefore different. The effect of this difference, however, is expected to be small, as it has been shown that the primary

https://doi.org/10.1017/jfm.2013.519 Published online by Cambridge University Press

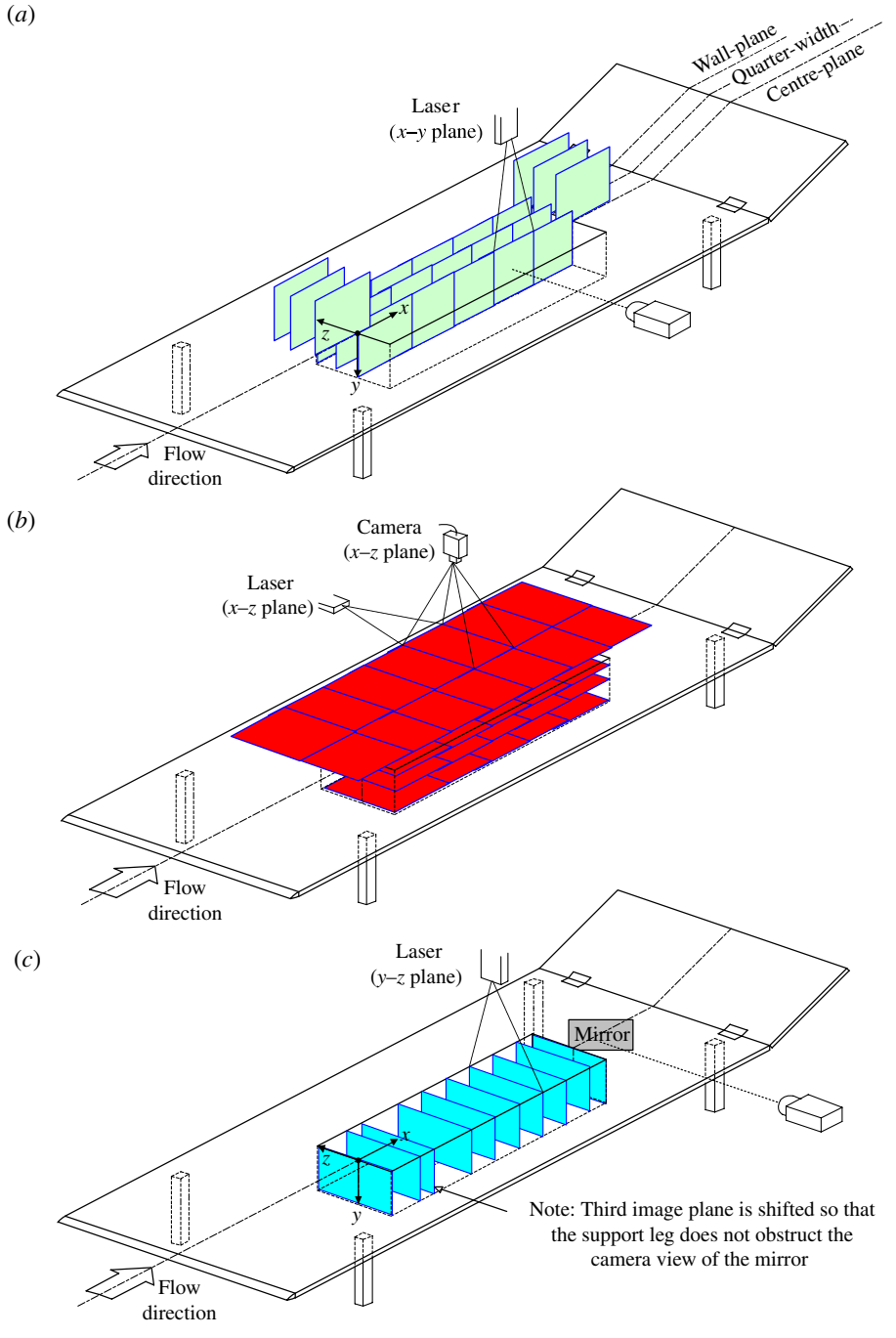


FIGURE 6. (Colour online) Sketch of all PIV imaging planes: (*a*) *x*–*y* planes measuring *u*, *v*; (*b*) *x*–*z* planes measuring *u*, *w*; (*c*) *y*–*z* planes measuring *v*, *w*.

parameter for similarity between experiments is the boundary layer thickness relative to the cavity dimensions (Rossiter 1964). The boundary layer type has been shown to have a negligible effect on cavity flow characteristics (Rossiter 1964; Reihman 1967).

https://doi.org/10.1017/jfm.2013.519 Published online by Cambridge University Press

Based on the methodology outlined by Raffel, Willert & Kompenhans (1998), the maximum error in the PIV velocity measurements was estimated to be approximately 9.2 % (which occurred at $x/d \approx 6$, $y/d \approx 0$). The mean error was found to be approximately 4 %.

3. Mean surface pressure distribution

3.1. *Three-dimensional pressure distribution*

Figure 7 shows the distribution of the time-averaged pressure coefficient on the internal surfaces of the cavity. It should be noted that where pressure tappings were available on both sides of the cavity, the time-averaged pressure measurements were approximately the same. This suggests that the time-averaged flow over the cavity is symmetric about the centre-plane. Therefore, data obtained on the left side of the cavity ($z+$) was reflected about the centre-plane onto the right side ($z-$) of the cavity.

On the front wall of the cavity, the pressure coefficient magnitudes are generally very low, ranging from -0.036 to -0.028. In fact, of all the cavity surfaces, the front wall has pressure coefficients which are closest to zero. This suggests that this region is devoid of any high velocity flow structures.

On the bottom surface of the cavity, a high pressure, high pressure gradient region exists towards the back of the cavity ($x/d \approx 5.4$–6.0). This is indicative of a downwash of high momentum fluid from the top to the bottom of the cavity near the back wall. Slightly upstream of this location, there is a low pressure region at $x/d \approx 3.5$–5.0. The low pressure is indicative of high velocity flow in this region. A local minimum of $C_p = -0.115$ occurs within this region along the cavity centreline. The remainder of the bottom surface experiences low magnitude negative pressure, which is consistent with the existence of a low velocity recirculation vortex (see also figure 3).

The results for the sidewalls are generally consistent with the pressure measurements on the bottom surface. All three regions identified above, i.e. the high pressure region close to the back plate, the low pressure region at $x/d \approx 3.5$–5.0, and a low pressure magnitude region towards the front wall, are consistently observed on the sidewalls.

On the side support plate (see figure 7), the most significant observation is the low pressure region at $x/d \approx 3.5$–5.0, corresponding to roughly the same region on both the sidewall and the bottom surface.

On the back wall, the entire surface experiences positive pressure, due to the fact the back wall is exposed to the approaching high momentum flow, similar to a forward-facing step (e.g. Stallings & Wilcox 1987). In contrast, the front wall is exposed to an almost quiescent region similar to a rearward-facing step. The peak pressure on the back wall is $C_p = 0.4$, occurring near the top of the cavity ($y/d \approx 0.1$) along the cavity centreline. This peak is the highest pressure observed within the cavity and is probably due to impingement of the shear layer onto the back wall. Therefore the location of this pressure peak should correspond to the location of a stagnation point. It is noted that the measured pressure coefficient of $C_p = 0.4$ at this stagnation point is much less than the free-stream dynamic pressure ($C_p = 1$). This is because the fluid in the shear layer that eventually stagnates on the cavity back wall originates from the upstream boundary layer, where fluid velocities are lower than the free-stream velocity.

Interestingly, the back wall experiences two local minima of $C_p = 0.1$ occurring at $y/d = 0.75$. Unlike the local maxima/minima on other surfaces, these local minima do not occur along the cavity centreline, but instead at $z/d = \pm 0.5$. Along the same depth at the centreline, the pressures tend to zero, suggesting that these local minima

https://doi.org/10.1017/jfm.2013.519 Published online by Cambridge University Press

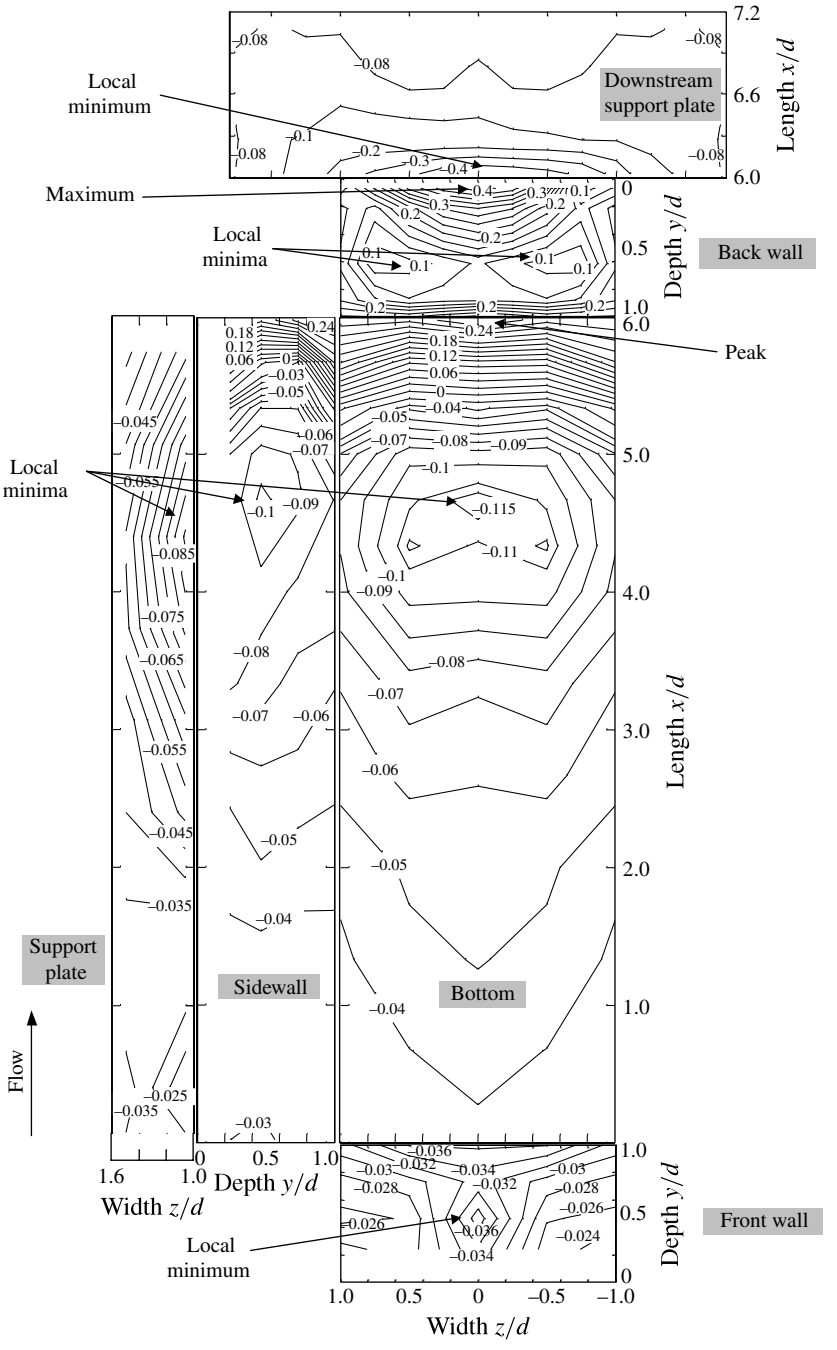


FIGURE 7. Surface pressure coefficient contours. Note that contours are not evenly separated.

correspond to regions of high fluid velocity, possibly decelerating towards a sink, or accelerating from a source, located approximately at the centre of the back wall.

On the downstream support plate, a low pressure region is observed close to the junction between the support plate and the back wall. This low pressure region only

https://doi.org/10.1017/jfm.2013.519 Published online by Cambridge University Press

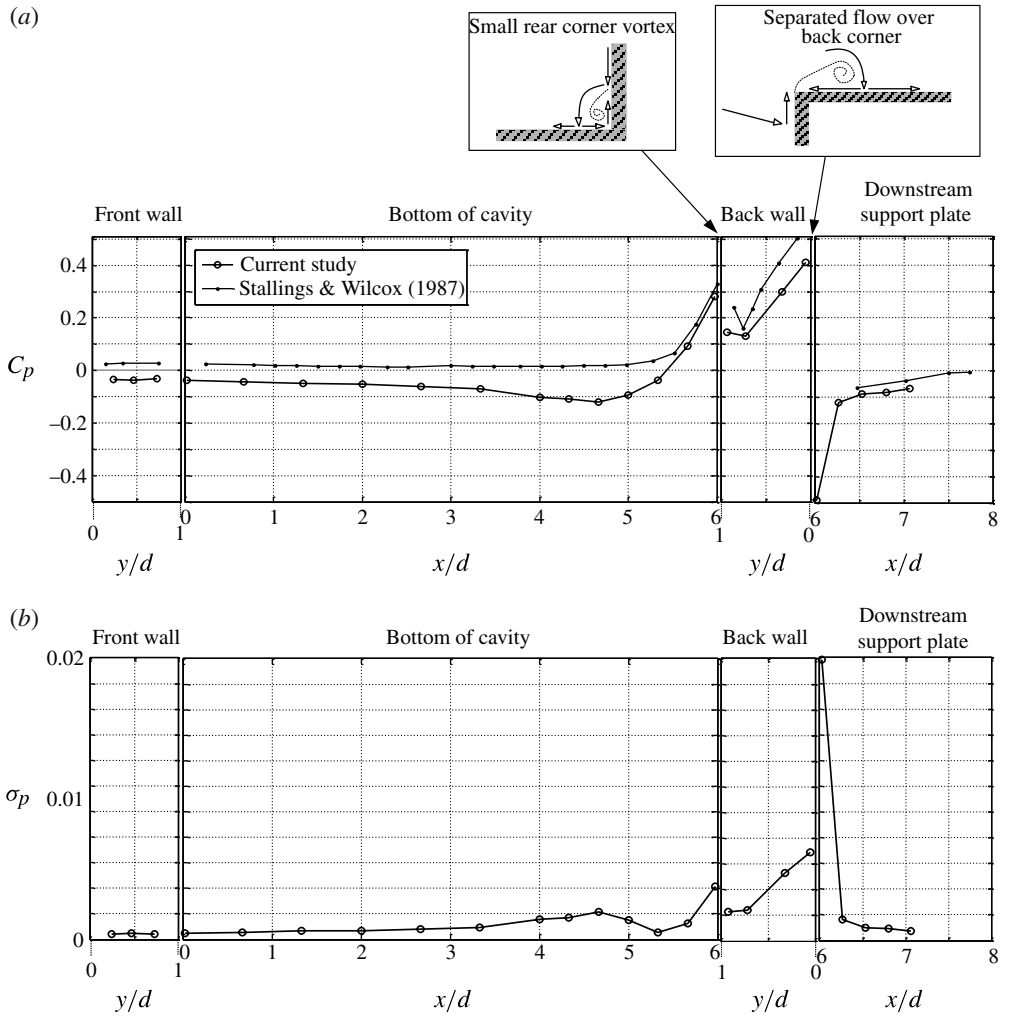


FIGURE 8. Mean pressure distribution (*a*) and standard deviation (*b*) along the centreline of the cavity.

extends a short distance downstream ($x/d \approx 6.0$–6.2), but spans the entire width of the cavity. The lowest pressure recorded on or around the cavity, $C_p = -0.4$, occurs within this region along the cavity centreline. This region is consistent with the presence of flow separation along the back corner of the cavity.

3.2. *Centreline pressure distribution*

Figure 8(*a*,*b*) shows the time-averaged pressure distribution and corresponding values of σ_P along the centreline of the cavity for the front wall, bottom, back wall and downstream support plate of the cavity. A comparison between the current experiments and those of Stallings & Wilcox (1987) for l:w:$d = 6$:1.25:1 and $M = 1.5$ indicates that the pressure distributions are generally similar. The most significant discrepancy is the existence of the low pressure region at $x/d = 3.5$–5.0 in the current experiment, which may be attributed to Mach number effects.

https://doi.org/10.1017/jfm.2013.519 Published online by Cambridge University Press

This low pressure region exhibits a relatively high σ_P, indicating a high degree of low frequency unsteadiness, consistent with the notion of a rear vortex whose position fluctuates with time. A high value of σ_P is also observed at the top of the back wall, corresponding to the expected location of a stagnation point. The relatively high values of σ_P at this location are indicative of fluctuations in the shear layer impingement location, leading to large variations in the local pressure coefficient. This fluctuation in the stagnation point location will also result in a time-averaged pressure coefficient that is lower than the free-stream total pressure, which provides an additional reason as to why the pressure at this point ($C_p = 0.4$) is significantly lower than the free-stream dynamic pressure.

Interestingly, a dip in pressure occurs on the back wall close to the bottom of the cavity ($y/d \approx 0.25$). This is possibly a sign of a small rear corner vortex, as shown in the inset of figure 8. A very high fluctuation in pressure occurs on the downstream support plate, close to the junction of the back wall, where the measured pressures are low. This is consistent with a high degree of unsteadiness in the separated flow over the back wall of the cavity.

4. Mean velocity distribution and internal flow structure

In the previous section, surface pressure measurements made within and around the cavity were used to infer basic flow structures. In this section, velocity fields consisting of multiple locations at three orthogonal planes within and around the cavity were used to directly plot fluid streamlines, velocity magnitude contours, and velocity fluctuation contours (in terms of σ_V). These were subsequently used in conjunction with the surface pressure measurements to construct an overall three-dimensional flow topology. It was not feasible to include all streamline patterns as well as velocity magnitude and fluctuation contours in this paper. Instead, we present only the time-averaged streamline patterns for all investigated planes, and discuss the individual flow features that have been identified largely based on these streamlines. These time-averaged streamline patterns for planes x–y, x–z and y–z are shown in figures 9, 10 and 11 respectively.

Figure 9 shows the time-averaged streamlines within the cavity for the x–y plane at $z/d = 0$, $z/d = 0.5$ and $z/d = 0.98$. In all three x–y planes, the *shear layer* which develops at the front corner of the cavity is observed to impinge on the back wall at $y/d \approx 0.1$–0.2. The location of this stagnation point is slightly lower than observed in the surface pressure measurements. This small discrepancy may be due to the different Reynolds numbers and initial boundary layer profiles in these experiments.

The fluid above the rear stagnation point appears to flow over the back wall, while the fluid below the stagnation point is drawn down towards the bottom of the cavity. The shear layer impingement can also be clearly seen in the flow pattern on the back wall (figure 11*j*). The impingement is identified by a series of critical points at $y/d \approx 0.13$, namely two half-saddles at the cavity sidewalls, a saddle on the cavity centreline, and two unstable nodes either side of the cavity centreline. This distribution of critical points is also consistent with the flow pattern close to the cavity back wall in the x–z plane ($x/d = 6.0$, figure 10*b*).

The shear layer is also seen to have a small ‘dip’ towards the bottom of the cavity at $x/d \approx 5.0$, as seen in figure 9. This dip manifests itself as a positive bifurcation on the y–z plane at $x/d = 5.33$ (figure 11*i*).

A commonly used measure of the shear layer growth rate is the length scale known as the vorticity thickness (Ashcroft & Zhang 2005; Haigermoser *et al.* 2008*b*),

https://doi.org/10.1017/jfm.2013.519 Published online by Cambridge University Press

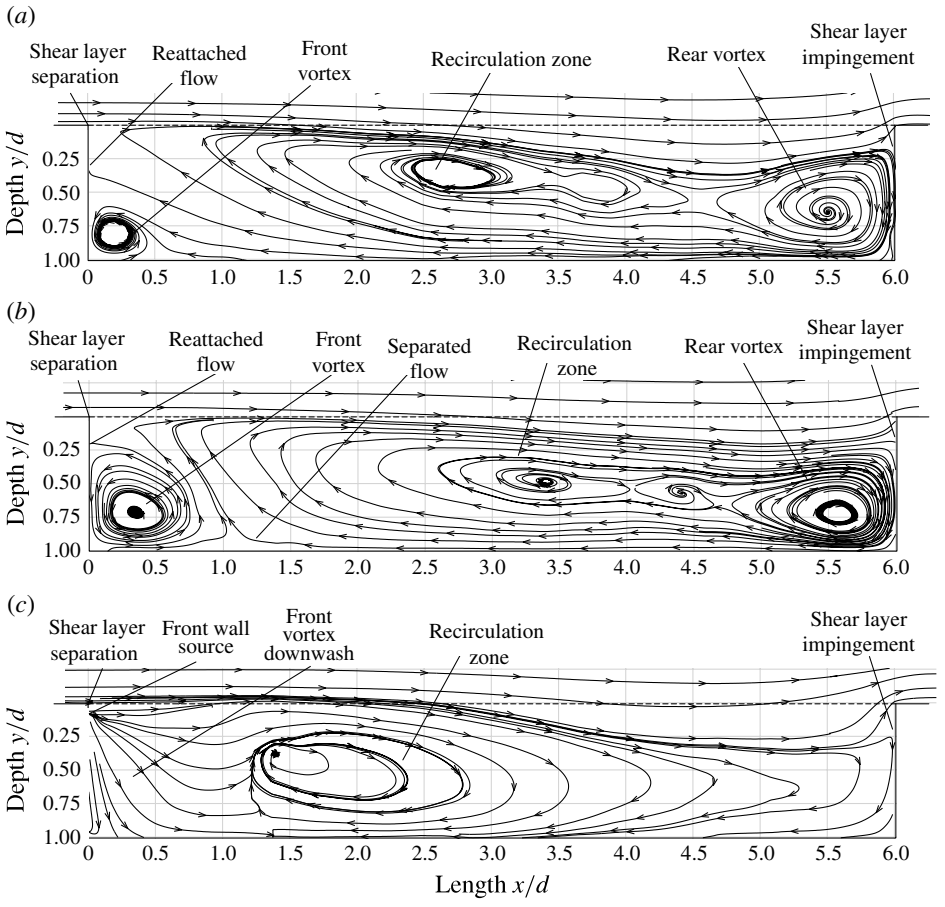


FIGURE 9. Time-averaged streamlines in the x–y plane at (a) $z/d = 0$, (b) $z/d = 0.5$ and (c) $z/d = 0.98$.

defined as

$$\delta_\omega(x) = \frac{U_\infty - U_c}{(\partial \overline{u}(x)/\partial y)}, \tag{4.1}$$

where $U_c \approx 0$ is the flow velocity within the cavity, and $\overline{u}$ is the x-component of the time-averaged velocity. Equation (4.1) assumes that the shear layer is perfectly planar and has zero transverse flow. While this has already been shown to be strictly invalid, the parameter δ_ω can still be used as an indicator of shear layer vorticity thickness.

Figure 12 shows the vorticity thickness, normalized to cavity length, as a function of streamwise distance. The results for all three x–y planes indicate that the vorticity thickness grows exponentially with distance up to $x/d \approx 1.5$. At $x/d \gtrsim 1.5$, the vorticity thickness along the centre-plane ($z/d = 0$) grows approximately linearly with streamwise distance. This result is consistent with the findings of Ashcroft & Zhang (2005) in two-dimensional cavity flow experiments, whereby the vorticity thickness was found to grow linearly with streamwise distance, resulting in a growth rate of $\partial\delta_\omega/\partial x \approx 0.143$. The latter result is also included in figure 12, and shows good agreement with the current experiments.

https://doi.org/10.1017/jfm.2013.519 Published online by Cambridge University Press

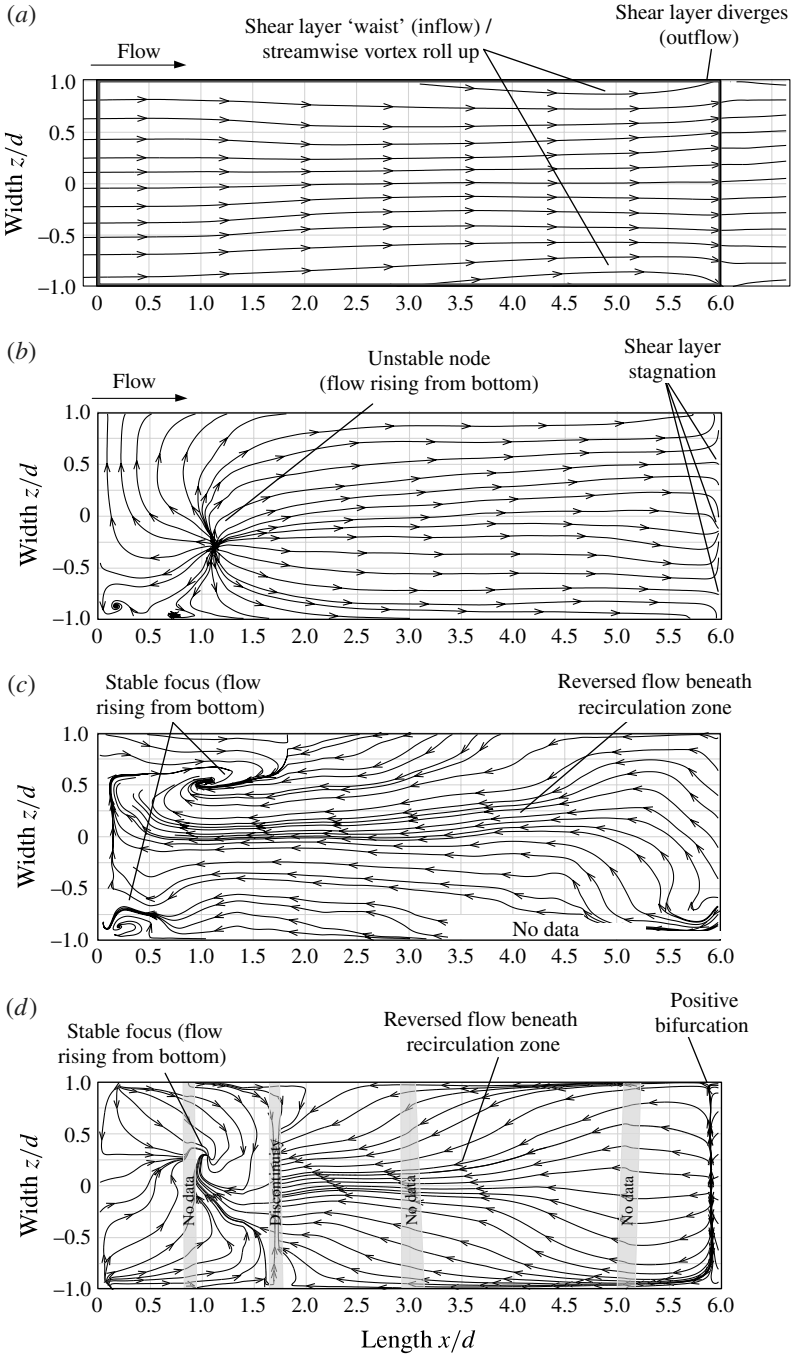


FIGURE 10. Time-averaged streamlines in the x–z plane at (*a*) $y/d = -0.03$, (*b*) $y/d = 0.15$, (*c*) $y/d = 0.7$ and (*d*) $y/d = 0.96$.

Ashcroft & Zhang reported results for an initially turbulent boundary layer, whereas in the present case, the incoming boundary layer was laminar ($H = 2.48$). By comparison, other studies obtained a range of results, presumably depending on

https://doi.org/10.1017/jfm.2013.519 Published online by Cambridge University Press

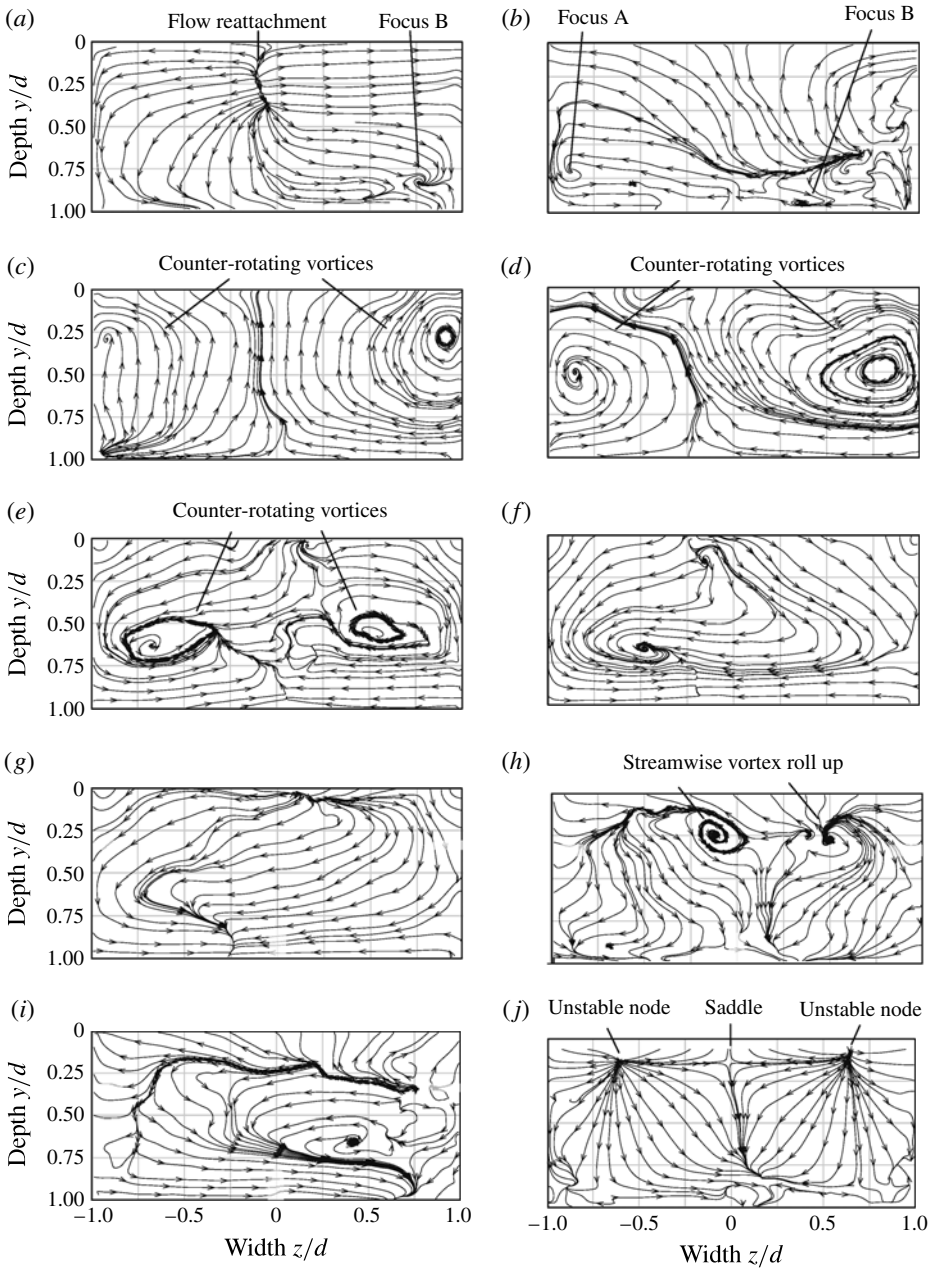


FIGURE 11. Time-averaged streamlines in the y–z plane at (*a*) $x/d = 0.03$, (*b*) $x/d = 0.66$, (*c*) $x/d = 1.00$, (*d*) $x/d = 2.00$, (*e*) $x/d = 2.66$, (*f*) $x/d = 3.33$, (*g*) $x/d = 4.00$, (*h*) $x/d = 4.66$, (*i*) $x/d = 5.33$ and (*j*) $x/d = 5.98$.

other factors such as Reynolds number and cavity geometry. This includes studies by Haigermoser *et al.* (2008*b*), Bian *et al.* (2011) and Ukeiley & Murray (2005), which reported vorticity thickness growth rates of $\partial\delta_\omega/\partial x \approx 0.19$, $\partial\delta_\omega/\partial x \approx 0.22$ (decreasing to 0.11), and $\partial\delta_\omega/\partial x \approx 0.12$ respectively. A study reporting both laminar and turbulent

https://doi.org/10.1017/jfm.2013.519 Published online by Cambridge University Press

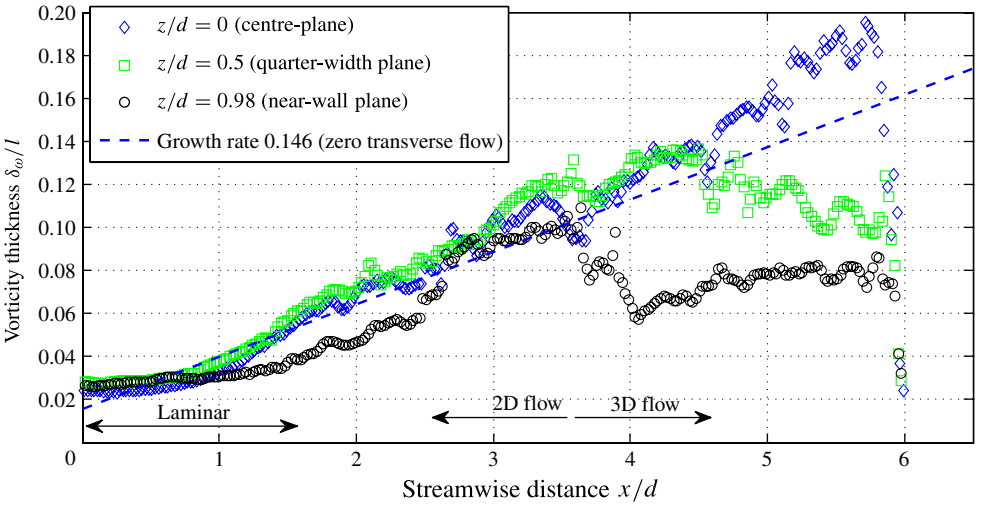


FIGURE 12. (Colour online) Shear layer vorticity thickness.

incident boundary layers was reported by Haigermoser *et al.* (2008*a*), showing both lower growth rates for initially laminar shear layers, and a parabolic increase with streamwise distance. A similar characteristic is shown in the present data, with a low initial growth rate, increasing to a relatively linear rate beyond $x/d \approx 1.5$.

At off-centre locations, the vorticity growth rate is found not to persist all the way to the end of the cavity, but appears to show a significant reduction at $x/d \approx 4.5$ and $x/d \approx 3.6$ for the quarter-width ($z/d = 0.5$) and near-wall ($z/d = 0.98$) plane respectively. This apparent three-dimensional effect may be related to the development of spanwise flow from the side-plate boundary layer, which encroaches laterally into the shear layer towards the back of the cavity.

Further evidence of this spanwise flow can be seen in the x–z plane a short distance above the top of the cavity (figure 10*a*), where the flow is seen to converge slightly towards the cavity centreline between $x/d \approx 3.5$–6.0. This convergence also corresponds to the low pressure region observed in the surface pressure measurements on the side support plate (see figure 7). Comparison of figure 10(*a*) with figure 10(*b*) and figure 11 shows that a short distance below the top of the cavity ($y/d \approx 0.15$) the flow diverges away from the centreline along the entire cavity length. Together, these observations suggest a complex structure in the flow at or above the edges of the cavity, consistent with a pattern of streamwise vortices lying approximately parallel to the cavity edges.

A clockwise *recirculation zone* is clearly visible in all three x–y planes (figure 9). This recirculation zone occupies approximately 60–90 % of the cavity length (depending on z) and covers almost the full width and depth. This feature, along with the shear layer that transverses the entire cavity length, is a defining feature of open-type cavity flows (see figure 2). The relative velocity magnitudes (in the x–y plane) range from $\approx 0.1U_\infty$ near the cavity bottom and sidewalls to $\approx 0.5U_\infty$ near the shear layer along the cavity centreline.

The core of the recirculation zone is a spanwise vortex originating at the cavity sidewalls. This is evidenced by the clockwise stable focus on the near-wall plane (figure 9*c*), at $x/d \approx 1.4$ and $y/d \approx 0.4$, which is consistent with a vortex attachment

https://doi.org/10.1017/jfm.2013.519 Published online by Cambridge University Press

point. This recirculation vortex appears to draw fluid from the sides of the cavity towards the cavity centreline. Within the recirculation zone on the bottom of the cavity, the flow direction is reversed relative to the free stream. The reversed flow is also visible in the x–z plane close to the bottom of the cavity (figure 10*d*). In this figure, a positive bifurcation line is observed very close to the back wall of the cavity ($x/d \approx 5.8$).

The streamline patterns observed in a study by Ruderich & Fernholz (1986) over a wide bluff body with a long splitter plate (similar to a backward-facing step) show good agreement with the observations above. Moreover, the flow pattern obtained by Dolling *et al.* (1997) in a hypersonic cavity flow also indicates similar reversed flow and bifurcation topology on the bottom surface of their cavity. However, the results of Dolling *et al.* do not support the observation that the recirculation vortex originates at the sidewalls. Instead, they report that the recirculation vortex originates from the shear layer impingement on the back wall.

In the x–y plane, the location of the recirculation core varies across the cavity, indicating that this spanwise vortex core is not normal to the sidewalls across the entire cavity width. In fact, the streamlines between $x/d \approx 1.5$–4.0 at the bottom of the cavity in the x–z plane (figure 10*d*), which are observed to converge towards the cavity centreline, suggests that the spanwise recirculation vortex is stretched in the downstream direction. This curved vortex core manifests itself as a pair of counter-rotating vortices in the y–z cross-sections, as seen in figure 11(*d*–*f*) ($x/d = 2.00$, 2.66 and 3.33).

Based on the positive bifurcation line on the bottom surface close to the back wall as shown in figure 10(*d*), we speculate on the existence of a *small rear corner vortex* located at the junction of the back wall and the bottom of the cavity. This is further supported by the rising flow at the base of the back wall (figure 11*j*), as well as the surface pressure measurements (see § 3). This small vortex appears to extend spanwise towards the sidewalls of the cavity. This interpretation is also supported by similar studies by Dolling *et al.* (1997). Dolling *et al.* go on to suggest that the ends of the small rear corner vortex turn upstream and transport fluid towards the front of the cavity where the pressure is lower. In the present study, the pattern provided in figure 11(*j*) also suggests that the ends of the vortex turn upstream, as indicated by the rotation direction of the foci on the lower left and right corners of the back wall ($y/d \approx 0.9$, $z/d \approx \pm 0.9$). The streamlines on the back wall of the cavity suggest that the small rear corner vortex draws fluid towards the cavity centreline for $-0.9 < z/d < 0.9$. Unfortunately, no other evidence of this vortex is observed in the velocity streamlines, possibly due to the small size and apparent strength of this vortex.

The centre and quarter-width image planes of the x–y plane (figure 9*a*,*b*) show a clockwise *rear vortex* at the back of the cavity, occupying approximately 20 % of the cavity length. This rear vortex appears to correspond to the low pressure region observed on the bottom surface in the surface pressure measurements (see figure 7). However, this low pressure region occurs at $x/d \approx 4.5$, while the velocity streamlines indicate that the centre of the rear vortex corresponds to $x/d \approx 5.5$. This discrepancy is attributed to the difference in Reynolds number and boundary layer type between the two experiments.

In the x–y plane, the rear vortex appears as an unstable focus spiralling fluid slowly outwards at the quarter-width plane and rapidly outwards at the centre-plane. Flow continuity dictates that the vortex (between the quarter-width plane and the wall-plane) must entrain fluid, then transport it towards the centre-plane of the cavity, i.e. along

https://doi.org/10.1017/jfm.2013.519 Published online by Cambridge University Press

the axis of the vortex towards the centre-plane. This agrees with the flow pattern in the y–z plane adjacent to the back wall (figure 11*j*). The transport of fluid from the sidewalls towards the centre of the cavity, and from the impinging shear layer downwards towards the cavity bottom, leads to high velocity flow on the back wall in the region of $y/d \approx 0.4$–0.6 and $z/d = \pm 0.4$–0.6 (figure 11*j*). This region of high velocity flow is consistent with the pressure minima measured in the surface pressure measurements (figure 7).

The absence of the rear vortex in the near-wall x–y plane (figure 9*c*) and the streamline pattern on the back wall (figure 11*j*) suggest that, on average, the vortex curves upwards near the back wall corners. Once the vortex approaches the shear layer, it is speculated that the vortex turns over the back corners and trails downstream of either side of the cavity. The adjacent surface flow pattern (figure 11*h*,*i*) suggests that the vortex transports fluid over the back wall of the cavity and into the free stream.

At the front of the cavity in the centre and quarter-width x–y planes (figure 9*a*,*b*), a *front vortex* is observed occupying approximately 10 % of the cavity length. The core of this vortex is located at $x/d \approx 0.20$–0.25 and $y/d \approx 0.75$–0.85. This vortex appears to be spiralling fluid inwards on average at the centre-plane, but outwards at the quarter-width plane, suggesting a weak lateral flow from the centre-plane of the recirculation zone towards the cavity sidewalls in this region. The front vortex appears to be relatively weak, having average flow velocities in its vicinity of approximately $0.03U_\infty$. A weak front vortex is consistent with the low magnitude surface pressures measured at the cavity front wall (see figure 7). The front vortex resides below a streamline that reattaches to the front wall (see figure 9*a*,*b*). The reattachment point is also clearly seen in the y–z plane close to the front wall (figure 11*a*). This reattachment point should, theoretically, coincide with a pressure peak on the cavity front surface. However, no pressure peak was observed (see figure 7).

The absence of the front vortex in the near-wall x–y plane (figure 9*c*) suggests that the vortex is not anchored to the sidewalls and must curve away from the sidewalls. There is no evidence that the vortex turns upstream and attaches to the front wall. However, there is evidence in figure 11(*b*,*c*) in the y–z plane that the vortex turns upward and downstream, as seen by the counter-rotating foci. These counter-rotating vortices are not to be confused with the similar counter-rotating recirculation vortices seen in figure 11(*d*,*e*); the front counter-rotating vortices occur upstream of the recirculation vortex anchor point on the cavity sidewall. This evidence suggests that the front vortex extends upwards towards the shear layer and subsequently downstream, where it is entrained into the shear layer and recirculating flow. The downwash on the sidewall in figure 9(*c*) (labelled 'front vortex downwash'), which does not appear in any other x–y plane, is consistent with the path of the turned vortex. Furthermore, the fluid on the bottom of the cavity (figure 10*d*) near the front wall ($x/d \approx 0.0$–1.5) appears to flow downstream and towards the cavity centreline, which is also consistent with the predicted turning of the front vortex.

The small-scale embedded foci seen downstream of the recirculation vortex in the x–y centre and quarter-width planes (figure 9*a*,*b*) may correspond to the front vortex loop which has been pulled downstream by the shear layer and then into the cavity by the recirculation vortex. This suggests that the front vortex line creates a closed loop within the cavity itself. This specific feature has not been observed by other researchers. It is possible that this feature may be specific to the Reynolds number ($Re_l = 4.3 \times 10^4$) and cavity geometry in the present experiments and is not a universal feature of cavity flows.

https://doi.org/10.1017/jfm.2013.519 Published online by Cambridge University Press

The rotation of the foci in the x–y plane correspond to the rotation of the two counter-rotating vortices observed in the y–z plane at $x/d = 4.77$ (figure 11*h*). These vortices, however, are located downstream of the embedded foci, resulting in a closed vortex loop that is pinched upstream at the cavity centreline. It should be noted that the recirculating vortex line also portrays this similar upstream 'pinch', suggesting a low pressure region and/or a significant flow feature between $x/d \approx 1.0$–2.0 close to the cavity centreline.

In the x–z plane near the bottom of the cavity (figure 10*d*), the flow in the region of $x/d \approx 0.0$–1.5 appears to be spiralling towards a single stable focus at $x/d \approx 1.0$, $z/d \approx 0.25$. This is evidence of a vortex structure which entrains fluid from both the recirculating vortex and the front vortex. This structure, which we shall call the *tornado-like vortex* due to its similarity in physical appearance to tornadoes, is also clearly seen in figure 10(*b*,*c*). In figure 10(*b*), the fluid entrained on the bottom of the cavity (close to or within the recirculation zone) by the tornado-like vortex is expelled close to the bottom of the shear layer. This tornado-like vortex appears to show significant lateral movement or bending in the z axis, but no noticeable variation in the longitudinal (x) axis. A similar vortex structure was observed by Atvars *et al.* (2009) in their CFD calculations for very narrow cavities with $w/d = 1$.

It is interesting to note that the region where the tornado-like vortex appears to reside also corresponds to the region where reversed flow on the bottom of the cavity is lifted towards the shear layer (figure 9*a*,*b*). The lifted flow is particularly pronounced at $x/d = 0.5$. This region of rising flow extends for at least half the width of the cavity, which also corresponds to the extent of the lateral movement or 'bending' of the tornado-like vortex (as seen in figure 10*c*).

In figure 10(*b*,*c*), evidence of a second tornado-like vortex of opposite rotational direction can be observed at $z/d \approx -0.9$. This tornado-like vortex, however, appears to be relatively weak in comparison with the above-mentioned feature. As the cavity itself is symmetric, the strengths of both tornado-like vortices should be equal. In fact, the 'pinching' of the recirculation and upstream section of the front vortex lines implies the existence of two counter-rotating tornado-like vortices located symmetrically about the cavity centreline. The existence of two counter-rotating tornado-like vortices would be consistent with Ruderich & Fernholz (1986), Wilcox (1992), Dolling *et al.* (1997) and Atvars *et al.* (2009), who observed two symmetric counter-rotating tornado-like vortices developing from the separated reversed flow on the bottom of their cavities or separation zones.

Interestingly, the rotational direction of the tornado-like vortices observed by Wilcox (1992) for $l/d = 10$, consistent with the current study, is opposite to that of the tornado-like vortices observed for cavities with $l/d \leqslant 5$ (Dolling *et al.* 1997; Atvars *et al.* 2009). This may indicate that the current cavity, with $l/d = 6$, lies within a transitional regime where the tornado-like vortices are unstable. This instability may cause the relative strengths and positions of the two counter-rotating tornado-like vortices to change, either periodically or randomly, with time scales that are much larger than the experimental sampling time. This theory is further supported by observations of the instantaneous flow field (not shown here), which indicates that the asymmetries in the cavity flow may switch from one extreme to another. Alternatively, it is also possible that within this transitional regime, the formation of these tornado-like vortices is sensitive to small asymmetries in the cavity geometry or the free-stream velocity profile, which will lead to significant asymmetries in the development of these tornado-like vortices. In either case, further evidence is required to resolve the evolution of the flow asymmetry.

https://doi.org/10.1017/jfm.2013.519 Published online by Cambridge University Press

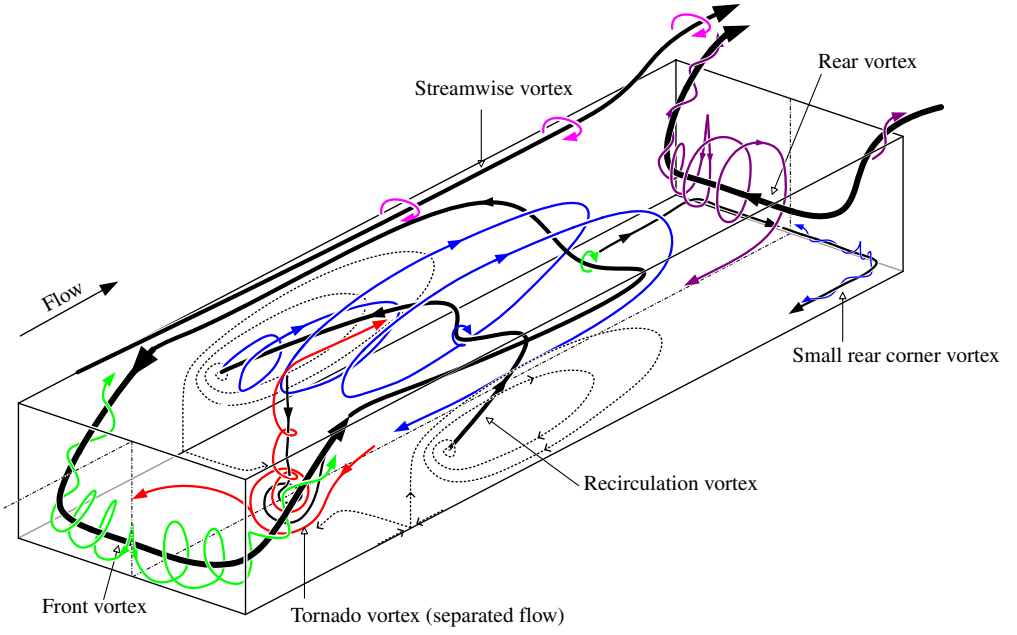


FIGURE 13. Diagrammatic summary of the time-averaged flow streamlines and vortex cores in an open-type cavity with l:w:d = 6:2:1.

The presence of this one dominant tornado-like vortex appears to be the primary source of flow asymmetry within the cavity. The asymmetric streamlines shown in figure 11(*f*,*g*), for example, are consistent with an asymmetrically deformed tornado-like vortex. The topology of all other cavity flow features, including the front and rear, streamwise, small rear corner and recirculation vortices are found to be reasonably symmetric about the cavity plane of symmetry. Therefore, the contribution of these features to the overall flow is expected to be symmetric about the cavity centre-plane.

A graphical representation of the flow patterns as well as vortex lines observed in the current study is shown in figure 13, while the surface flow patterns are summarized in figure 14. A two-dimensional cross-section of the cavity flow along the centre-plane is shown in figure 15. These results are topologically self-consistent, and show good agreement with both PIV velocity streamlines and surface pressure measurements.

5. Concluding remarks

In summary, the flow in and around a cavity with a geometrical ratio of l:w:d = 6:2:1 was investigated using surface pressure measurements ($Re_l = 3.4 \times 10^5$) and two-component PIV ($Re_l = 4.3 \times 10^4$). The results indicate that the time-averaged cavity flow is complex, containing several interacting vortical structures. These structures are summarized in figures 13–15. The results presented here are topologically self-consistent. There is good agreement with the direction of the flow and the velocity magnitude in the PIV data obtained in the three orthogonal planes. Generally there is also agreement between the surface-pressure measurements and the velocity field data. While the flow patterns formed within the present cavity are generally in agreement with the literature, the present study also reveals an asymmetric flow regime that has not previously been reported.

https://doi.org/10.1017/jfm.2013.519 Published online by Cambridge University Press

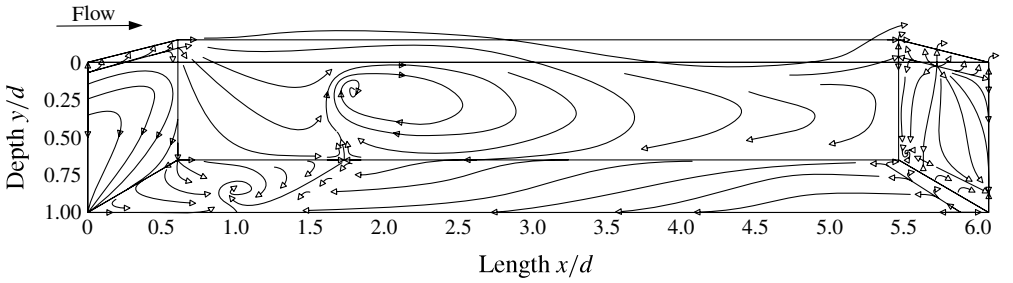


FIGURE 14. Cutaway view of the cavity, illustrating surface flow patterns observed in an open-type cavity with l:w:d = 6:2:1.

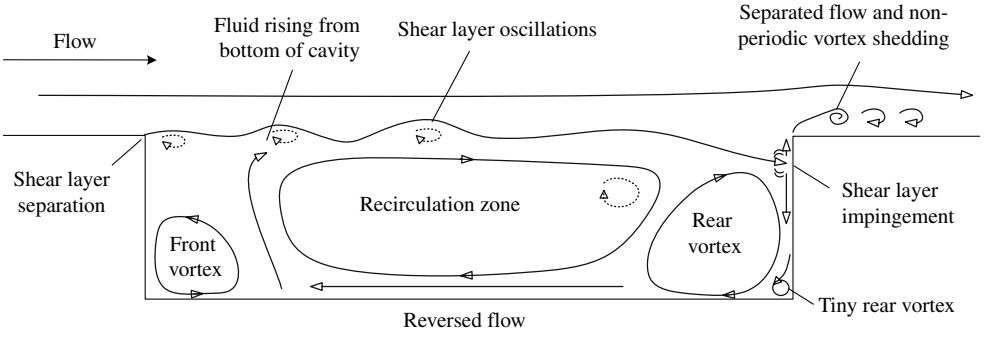


FIGURE 15. Diagram of the two-dimensional cross-section (along cavity centreline) of the time-averaged flow within a cavity with l:w:d = 6:2:1.

The present experiments show that the cavity flow is an open-type flow field, with a shear layer originating from the front edge of the cavity traversing the entire length of the cavity and a large internal cavity recirculation zone. The shear layer impinges on the back wall at $y/d \approx 0.1$–0.2. Surface pressure measurements suggests that this impingement point fluctuates with time.

The recirculation vortex encompasses approximately 70 % of the cavity length, and has velocity magnitudes in the range of 0.1–$0.5U_\infty$. This vortex spans the cavity and connects to the cavity sidewalls at $x/d \approx 1.4$ and $y/d \approx 0.4$. The recirculation vortex is not perpendicular to the sidewalls throughout the cavity, but is pulled downstream on either side of the cavity, leading to a backwards pinching effect at the cavity centreline.

Upstream of the recirculation vortex is a front vortex, positioned near the junction of the front and bottom cavity surfaces. This front vortex, which is of opposite rotational sense to the recirculation vortex, is relatively weak, with velocities in the range of 0.01–$0.04U_\infty$. The low pressure magnitudes on the front wall of the cavity are consistent with the existence of this low circulation vortex. The front vortex forms a closed loop within the cavity towards the downstream end, and also shows a pinching effect similar to the recirculation vortex.

Near the back wall of the cavity, a rear vortex occupies approximately 20 % of the cavity length. The velocity magnitudes within this vortex are in the range 0.05–$0.3U_\infty$, leading to a small reduction in surface pressure at the upstream region of the cavity

https://doi.org/10.1017/jfm.2013.519 Published online by Cambridge University Press

bottom. The rear vortex lines bend upwards parallel to the cavity back wall and then turn and trail off downstream.

Below this rear vortex, along the junction between the cavity bottom and back surfaces, a small rear corner vortex exists. This vortex was not observed directly due to its small size and proximity to the boundaries, but is inferred from surface pressure measurements as well as various critical points in the near-wall streamline patterns. It is postulated that the small rear corner vortex turns and extends upstream. The trajectory of this vortex beyond this point is unknown.

Two counter-rotating streamwise vortices, located at the upper corners of the sidewalls, are inferred from observations of the mean velocity field and surface pressure measurements near the cavity edges.

Upstream of the recirculation vortex lies a tornado-like vortex which appears to draw fluid from the bottom of the cavity, expelling it at the top of the cavity near the shear layer. The core of this vortex is attached to the bottom of the cavity at $x/d \approx 1.0$ and $z/d \approx 0.25$. The tornado-like vortex extends upwards towards the shear layer, where it presumably turns downstream. This tornado-like vortex does not show any evidence of streamwise motion, but appears to bend and deform in the lateral (z) direction. This vortex appears to be the primary indication of asymmetry within the flow.

There is some evidence of a second tornado-like vortex, of opposite rotational sense, close to the front of the cavity near the left (z^-) sidewall. This vortex, if it exists, is very weak. It is postulated that two counter-rotating tornado-like vortices of similar (absolute) strength do indeed exist in the cavity. However, these vortices are unstable, and thus have significant lateral motion within the cavity. More importantly, the relative strengths of these vortices are also time-dependent, such that the role of the dominant vortex changes with time. This results in overall flow asymmetry which switches from one extreme to another. This process, which may be periodic or random, is postulated to occur on time scales which are much larger than the sampling times of the current experiment, leading to what appears to be an asymmetric flow in the time-averaged data. If the sampling time of the current experiments were sufficiently large, we might expect the mean location of the tornado-like vortices to be symmetric about the cavity centreline, at $z/d \approx \pm 0.25$–0.75, as shown in figure 14. This would be consistent with the upstream pinching of the front and recirculation vortex lines.

The motion, deformation, and strength fluctuations of the individual tornado-like vortices imply that the instantaneous velocity field in and around the cavity is highly asymmetric and three-dimensional. It is postulated that the existence of this asymmetric mode is linked to the l/d ratio of the cavity, where the range $l/d \approx 5 - 10$ coincides with a transitional regime where the counter-rotating tornado-like vortices, as observed in the mean flow, switch from one rotational sense to another.

Acknowledgements

The authors would like to acknowledge Mr E. Hassan and Dr P. Lanspeary for their useful discussions and technical input.

REFERENCES

ASHCROFT, G. & ZHANG, X. 2005 Vortical structures over rectangular cavities at low speed. *Phys. Fluids* **17**, 015104.

ATVARS, K., KNOWLES, K., RITCHIE, S. & LAWSON, J. 2009 Experimental and computational investigation of an open transonic cavity flow. *J. Aerosp. Engng* **223**, 357–368.

https://doi.org/10.1017/jfm.2013.519 Published online by Cambridge University Press

BIAN, S., DRISCOLL, J. F., ELBING, B. R. & CECCIO, S. L. 2011 Time resolved flow field measurements of a turbulent mixing layer over a rectangular cavity. *Exp. Fluids* **51**, 51–63.

BRASLOW, A., HICKS, R. & HARRIS, 1966 Use of grit-type boundary-layer-transition trips on wind-tunnel models. NASA Technical Note D-3579.

CHARWAT, A. F., FOOS, J. N., DEWEY, F. C. & HITZ, J. A. 1961 An investigation of separated flows. Part 1. The pressure field. *J. Aero. Sci.* **28** (6), 457–70.

DIX, R. E. & BUTLER, C. 1990 Cavity aeroacoustics. *Tech. Rep.* A358322 Oct 85–Apr 90, Calspan Corporation, Arnold Engineering Development Center Operations, Arnold Air Force Base.

DOLLING, D. S., PERNG, S. W. & LEU, Y. L. 1997 An experimental study of passive control of hypersonic cavity flow oscillations. *Tech. Rep.* AFRL-SR-BL-TR-98-0240, Center for Aeromechanical Research, University of Texas, Austin.

EAST, L. F. 1966 Aerodynamic induced resonance in rectangular cavities. *J. Sound Vib.* **3** (3), 277–287.

FAURE, T., ADRIANOS, P., LUSSEYRAN, F. & PASTUR, L. 2007 Visualisation of the flow inside and open cavity at medium range Reynolds numbers. *Exp. Fluids* **42**, 169–184.

FORESTIER, N., JACQUIN, L. & GEFFORY, P. 2003 The mixing layer over a deep cavity at high-subsonic speed. *J. Fluid Mech.* **475**, 110–145.

HAIGERMOSER, C., SCARANO, F., ONORATO, M., TORINO, P. & DELFT, T. 2008*a* Investigation of the flow in a rectangular cavity using tomographic and time-resolved PIV. In *26th International Congress of the Aeronautical Science*, Anchorage, Alaska, 14–19 September 2008.

HAIGERMOSER, C., VESELY, L., NOVARA, M. & ONORATO, M. 2008*b* A time-resolved particle image velocimetry investigation of a cavity flow with a thick incoming turbulent boundary layer. *Phys. Fluids* **20**, 105101.

KARAMECHETI, K. 1956 Sound radiated from surface cutouts in high-speed flows. PhD thesis, California Institute of Technology.

KNOWLES, K., RITCHIE, S. & LAWSON, J. 2007 An experimental and computational investigation of a 3D, $l/h = 5$ transonic cavity flow. In *3rd International Symposium on Integrating CFD and Experiments in Aerodynamics*. US Air Force Academy.

LARCHEVEQUE, L., SAGAUT, P. & LABBE, O. 2007 Large-eddy simulation of subsonic cavity flow including asymmetric three-dimensional effects. *J. Fluid Mech.* **577**, 105–126.

LARCHEVEQUE, L., SAGAUT, P., LE, T.-H. & COMTE, P. 2004 Large-eddy simulation of a compressible flow in a three-dimensional open cavity at high Reynolds number. *J. Fluid Mech.* **516**, 265–301.

LARSSON, J. 2002 Computational aero acoustics for vehicle applications. PhD thesis, Chalmers University of Technology.

MANOVSKI, P., GIACOBELLO, J. & M. SORIA, 2008 Particle image velocimetry measurements over an aerodynamically open two-dimensional cavity. In *Proceedings of the 5th Australian Conference on Laser Diagnostics in Fluid Mechanics & Combustion, University of Western Australia, 3–4 December*.

MARY, I. & LE, T.-H. 2005 Large-eddy simulations of flow past weapons bay. In *AVT-123 Symposium on Flow Induced Unsteady Loads and The Impact of Military Applications*.

MAULL, D. & EAST, L. F. 1963 Three-dimensional flow in cavities. *J. Fluid Mech.* **16** (4), 620–632.

MILBANK, J. 2004 Investigation of fluid-dynamic cavity oscillations and the effect of flow angle in an automotive context using an open-jet wind tunnel. PhD thesis, RMIT University.

OZSOY, E., RAMBAUD, P., STITOU, A. & RIETHMULLER, M. 2005 Vortex characteristics in laminar cavity flow at very low Mach number. *Exp. Fluids* **38**, 133–145.

PLUMBLEE, H. E., GIBSON, J. S. & LASSITER, L. W. 1962 A theoretical and experimental investigation of the acoustic response of cavities in an aerodynamic flow. *Tech. Rep.* Wright-Patterson Air Force Base, Technical Report WADD-TR-61-75.

RAFFEL, M., WILLERT, C. & KOMPENHANS, J. 1998 *Particle Image Velocimetry: A Practical Guide*, 3rd edn. Springer.

REIHMAN, T. C. 1967 Laminar flow over transverse rectangular cavities. PhD thesis, California Institute of Technology.

https://doi.org/10.1017/jfm.2013.519 Published online by Cambridge University Press

ROSSITER, J. E. 1964 Wind tunnel experiments on the flow over rectangular cavities at subsonic and transonic speeds. Royal Aircraft Establishment, ARC Reports and Memoranda 3438.

RUDERICH, R. & FERNHOLZ, H. 1986 An experimental investigation of a turbulent shear flow with separation, reverse flow, and reattachment. *J. Fluid Mech.* **163**, 283–322.

SAROHIA, V. 1977 Experimental investigation of oscillations in flows over shallow cavities. *AIAA J.* **15** (7), 984–991.

STALLINGS, R. L. & WILCOX, F. 1987 Experimental cavity pressure distributions at supersonic speed. NASA Technical Paper 2683, Langley Research Centre, Hampton, Virginia.

THWAITES, B. 1949 Approximate calculations of the laminar boundary layer. *Aeronaut. Q.* **1**, 245–280.

TRACY, M. & PLENTOVISH, E. 1993 Characterization of cavity flow fields using pressure data obtained in the Langley 0.3-meter transonic cryogenic tunnel. NASA Technical Memorandum 4436, Langley Research Centre, Hampton, Virginia.

UKEILEY, L. & MURRAY, N. 2005 Velocity and surface pressure measurements in an open cavity. *Exp. Fluids* **38**, 656–671.

WESTERWEEL, J. & SCARANO, F. 2005 Universal outlier detection for PIV data. *Exp. Fluids* **36**, 1096–1100.

WILCOX, F. Jr 1990 Experimental measurements of internal store separation characteristics at supersonic speeds. In *Store Carriage, Integration and Release Conference*, pp. 5.1–5.16. Royal Aeronautical Society.

WILCOX, F. Jr 1992 Use of a coloured water flow visualization technique in a supersonic wind tunnel to investigate cavity flow fields. In *Flow Visualization VI: Proceedings of the Sixth International Symposium on Flow Visualization*, p. 4145 Springer.

YAO, H., COOPER, R. & RAGHUNATHAN, S. 2004 Numerical simulation of incompressible laminar flow over three-dimensional rectangular cavities. *Trans. ASME: J. Fluids Engng* **126**, 919–927.

ZDANSKI, P., ORTEGA, M., NIDE, G. & FICO, Jr 2003 Numerical study of the flow over shallow cavities. *Comput. Fluids* **32**, 953–974.

https://doi.org/10.1017/jfm.2013.519 Published online by Cambridge University Press